Journal of Materials Chemistry A

RSC Publishing

PAPER

View Article Online
View Journal | View Issue

Cite this: J. Mater. Chem. A, 2013, 1, 1220

Novel synthesis of $Li_{1.2}Mn_{0.4}Co_{0.4}O_2$ with an excellent electrochemical performance from −10.4 to 45.4 °C

Dong Luo,[a] Guangshe Li,[b] Xiangfeng Guan,[b] Chuang Yu,[a] Jing Zheng,[a] Xinhui Zhang[b] and Liping Li*[a]

Received 6th September 2012
Accepted 6th November 2012

DOI: 10.1039/c2ta00205a

www.rsc.org/MaterialsA

Lithium-ion batteries continue to dominate the market and transportation applications of portable electronics, while these applications are still very difficult at low or elevated temperatures. In this work, the cathode material $Li_{1.2}Mn_{0.4}Co_{0.4}O_2$ was initially synthesized *via* an oxalate-precursor method. During sample preparation, lithium ions were co-precipitated with transition metal ions to form a uniform distribution of reactants at the molecular level. As a consequence, the current preparation method gave rise to a uniform cation distribution inside the target materials with no need of the additional process of mixing with lithium salt, which is however always required when using conventional co-precipitation methods. Due to the uniform cation distribution inside the material, the $Li_{1.2}Mn_{0.4}Co_{0.4}O_2$ cathode thus prepared was found to exhibit an excellent electrochemical performance. At room temperature, the initial discharge capacity and capacity retention ratio after 20 cycles were 284 mA h g^{-1} and 82.75%, respectively, which are superior to 246 mA h g^{-1} and 79.27%, the best results ever reported for the counterparts. Further, the low and elevated-temperature electrochemical performance for this cathode was also explored. It was found that the maximal discharge capacity measured at a current density of 20 mA g^{-1} between 2.0 and 4.6 V was maintained as high as 296 and 200 mA h g^{-1}, at 45.4 and −10.4 °C, respectively. The change in the state of health (SOH) in the temperature range −10.4 to 45.4 °C was investigated by EIS. It was demonstrated that the %SOH operation window for $Li_{1.2}Mn_{0.4}Co_{0.4}O_2$/Li cells was somewhat broad, which indicated a potential application at low/elevated temperatures. The synthetic route described in this work is new, and may help to prepare more advanced cathode materials essential for a broad class of applications.

1 Introduction

Nowadays, lithium-ion batteries continue to dominate the market and transportation applications of portable electronics, which drives researchers and engineers to build better batteries.[1–3] It is well established that battery performances are directly determined by the electrode materials, and that the synthesis routes to the relevant materials affect the structure of the electrode materials during the charge and discharge cycles of the batteries. Consequently, many synthetic methods have been developed to prepare cathode materials, including solid-state reactions,[4] molten-salt routes,[5] co-precipitation methods,[6] and others.[7] Despite some progress in the right direction, the preparation of cathode materials still faces great challenges, one of which is how to achieve a cathode material with an excellent electrochemical performance that allows lithium-ion batteries to operate at low or elevated temperatures.

To meet these challenges, two priorities are necessary: (i) raw materials should be mixed uniformly, in particular at the molecular level, and (ii) the involvement of unwanted metal-ion impurities in the precursors has to be avoided. Such a task appears very difficult, since some preparation methods (*e.g.*, the molten-salt route) can achieve uniform mixing of raw materials at the molecular level, while the mineralizers (*e.g.*, NaOH or KOH) essential for the crystallization of the final products usually introduce certain metal-ion impurities, *e.g.*, K^+ or Na^+. These metal-ion impurities, no matter whether they are in the internal lattice or at the surface, would have an impact on the electrochemical performances of the electrode materials. On the other hand, using LiOH, NH_4HCO_3, and $(NH_4)_2C_2O_4$ instead of NaOH as a precipitant could avoid the introduction of impurity ions into the precursors of the transition metal salts.[8–10] Nevertheless, Li^+ ions cannot be precipitated by any of the above precipitants in an aqueous solution. Namely, Li^+ ions cannot be co-precipitated with transition metal ions. As a result, a subsequent process of mixing with lithium salts has to be used, which leads to an uneven distribution of lithium salts in

[a]Key Lab of Optoelectronic Materials, Chemistry and Physics, Fujian Institute of Research on the Structure of Matter, University of Chinese Academy of Sciences, Fuzhou 350002, P. R. China. E-mail: lipingli@fjirsm.ac.cn

[b]State Key Laboratory of Structural Chemistry, Fujian Institute of Research on the Structure of Matter, University of Chinese Academy of Sciences, Fuzhou 350002, P. R. China

the precursors and furthermore some uncontrolled side reactions and a decreased reaction rate. Therefore, exploring a novel route that allows lithium ions to be co-precipitated with transition metal ions without the introduction of impurity ions is extremely important for the development of lithium-ion batteries for a broad class of applications.

Very recently, we prepared $LiCoO_2$ doped with a low concentration of Mn^{4+} using a molten-salt route. It was found that the electrochemical performance of the $LiCoO_2$ cathode was greatly improved,[11] while traces of Na^+ from the reactants were also introduced, which had some negative effects on the electrode performance. Herein, we aimed to decorate the surfaces of $LiCoO_2$ with Li_2MnO_3 to prepare a uniform composite electrode material $Li_{1.2}Mn_{0.4}Co_{0.4}O_2$ without introducing any metal-ion impurities. The electrode was expected to operate in a wide temperature range with an excellent electrochemical performance. For this purpose, we designed a new oxalate-precursor method to produce the cathode material $Li_{1.2}Mn_{0.4}Co_{0.4}O_2$ based on the following considerations: oxalic acid has an greater acidity than acetic acid, and the oxalate anion is more stable than the acetate anion. Thus, one can expect that when oxalic acid was added to an acetic acid salt solution, acetic acid and oxalate anions would be formed. Eventually, oxalate anions may react with all the metal-ions to form the oxalate precursors of multi-component cathode materials with an improved uniformity of reactants at the molecular level, as illustrated in Fig. 1. Then, a powder material $Li_{1.2}Mn_{0.4}Co_{0.4}O_2$ would be obtained by calcining the precursors of the metal oxalates at 900 °C. The results of electrochemical tests indicated that this new oxalate-precursor method is quite promising for the preparation of metal oxide cathode materials.

2 Experimental section

2.1 Sample synthesis

The $Li_{1.2}Mn_{0.4}Co_{0.4}O_2$ cathode material was prepared using a new oxalate-precursor method. The preparation procedure can be described briefly as follows: lithium acetate ($CH_3COOLi\cdot 2H_2O$), manganese acetate ($Mn(CH_3COO)_2\cdot 4H_2O$), and cobalt acetate ($Co(CH_3COO)_2\cdot 4H_2O$) were chosen as the starting materials, and ethanol was used as the solvent. 1285.5 mg of $CH_3COOLi\cdot 2H_2O$ (5 mol% excess), 980.4 mg $Mn(CH_3COO)_2\cdot 4H_2O$, and 996.4 mg $Co(CH_3COO)_2\cdot 4H_2O$ were dissolved together in 100 mL of ethanol, and 2163.4 mg of ethanedioic acid was dissolved in 30 mL of ethanol. After stirring for about 10–30 min, ethanedioic acid was added dropwise to the acetic acid salt solution to get the oxalate precursor. All these chemical reactions were carried out at room temperature. After filtering and sufficient washing, this precursor was calcined in air at 900 °C for 12 h and then quenched to room temperature to give the final product.

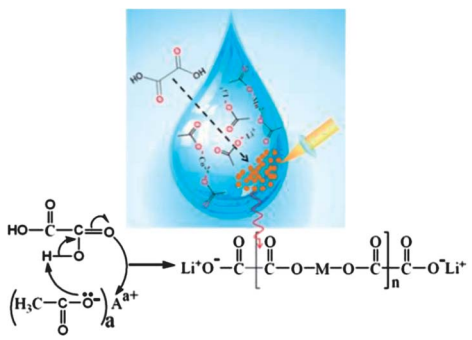

Fig. 1 Formation process proposed for the oxalate-precursor. A is Li, Mn, or Co and M is Mn or Co.

2.2 Sample characterization

The crystalline phases of the synthesized materials were identified by X-ray diffraction (XRD) on a Rigaku DESKTOP X-ray diffractometer using Cu Kα (λ = 1.5418 Å) radiation. Lattice parameters of the samples were calculated through structural refinements using the GSAS program with potassium chlorate as the internal standard for peak position calibration. The particle morphologies and sizes of the samples were determined by field emission scanning electron microscopy (SEM) on a JEOL JSM6700F instrument under an acceleration voltage of 5 kV. Thermal gravimetric analysis of the sample was conducted using a Netzsch thermo-analyzer STA449F3 at a heating rate of 10 °C min^{-1} in air over a temperature range of 30–1030 °C.

The chemical compositions of the samples were analyzed by Inductively Coupled Plasma Atomic Emission Spectrometry (ICP-AES). The valence states of the transition metal ions in the sample were determined by X-ray photoelectron spectroscopy (XPS) on ESCA-LAB MKII apparatus with a monochromatic Al Kα X-ray source. During the XPS measurements, the base pressure of the sample chamber was kept at less than 3.0×10^{-10} mbar. Emission lines were calibrated using the C 1s signal at 284.6 eV.

2.3 Electrochemical tests

The electrochemical performances of the samples were measured using a CR-2025-type coin cell. The cathode materials were prepared as follows: 80 wt% of the synthesized powders, 10 wt% of carbon black, and 10 wt% of polyvinylidene fluoride (PVDF) were mixed using *N*-methyl pyrrolidinone (NMP) as a solvent. The resulting slurry was coated on Al foil by a doctor blade technique and vacuum dried at 100 °C for 6 h. The cells were assembled in an argon-filled glove box (H_2O and O_2 <1 ppm) using lithium foil as the anode, a polymer separator and 1 M $LiPF_6$ in ethylene carbonate (EC) : ethyl methyl carbonate (EMC) : dimethyl carbonate (DMC) (1 : 1 : 1 by volume) as the electrolyte. The cell was charged and discharged galvanostatically in a voltage range of 2.0–4.6 V at −10.4, 25, and 45.4 °C with different current densities of 20, 60, 100, and 200 mA g^{-1}.

3 Results and discussion

The precursor had the formula $(Li_{1.2}Mn_{0.4}Co_{0.4})_x(C_2O_4)_y$ as indicated by chemical analysis. As shown in Fig. 2a, the precursor showed several broad diffraction peaks along with several sharp lines. Additionally, it was indicated that the

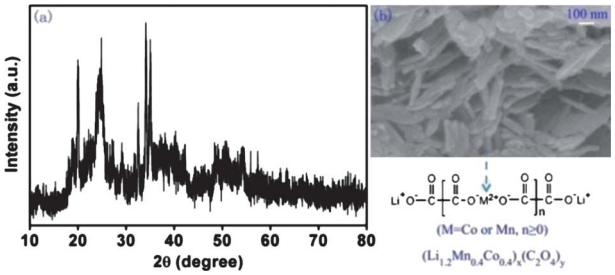

Fig. 2 (a) XRD pattern and (b) SEM image of the precursor, $(Li_{1.2}Mn_{0.4}Co_{0.4})_x(C_2O_4)_y$.

morphology of the precursor was wire shaped with a diameter of about 50 nm (Fig. 2b).

To understand the conversion of precursor into the $Li_{1.2}Mn_{0.4}Co_{0.4}O_2$ cathode material, the precursor was investigated by thermal gravimetric analysis (TG). Fig. 3 shows the TG, differential thermal gravimetry (DTG) and differential thermal analysis (DTA) curves of the precursor. The DTG curve shows that weight loss took place in three steps, which were modelled with Gaussian curves. The first weight loss step occurred between 130 and 287 °C and was ascribed to the sublimation and decomposition of oxalic acid ($H_2C_2O_4$) with 12.8% weight loss, and was accompanied by an exothermic peak at about 168 °C in the DTA curve. The second step involving 25.8% weight loss occurred between 287 and 307 °C and was attributed to the decomposition of MnC_2O_4 and some CoC_2O_4, and corresponds to an exothermic peak at about 304 °C in the DTA curve. The final step involving 16.1% weight loss occurred between 307 and 495 °C and was due to the decomposition of $Li_2C_2O_4$ and a small amount of CoC_2O_4. The DTA curve exhibits an endothermic peak at about 800 °C, which indicates that a layered structure of $Li_{1.2}Mn_{0.4}Co_{0.4}O_2$ was produced. In this work, we chose 900 °C as the synthesis temperature.

The microstructures of the sample were systematically examined by SEM, XRD, and XPS. As indicated by the SEM image in Fig. 4a, all particles were observed to have a uniform size with a diameter distribution in the range 300–500 nm. Fig. 4b shows the XRD pattern of the sample. The strong diffraction peaks are well indexed by the $R\bar{3}m$ structure of

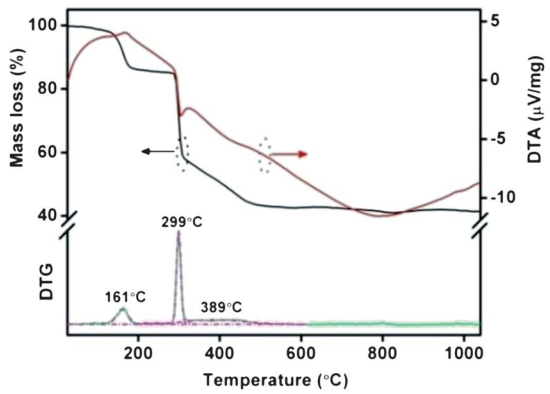

Fig. 3 TG, DTA and DTG curves of the precursor, $(Li_{1.2}Mn_{0.4}Co_{0.4})_x(C_2O_4)_y$.

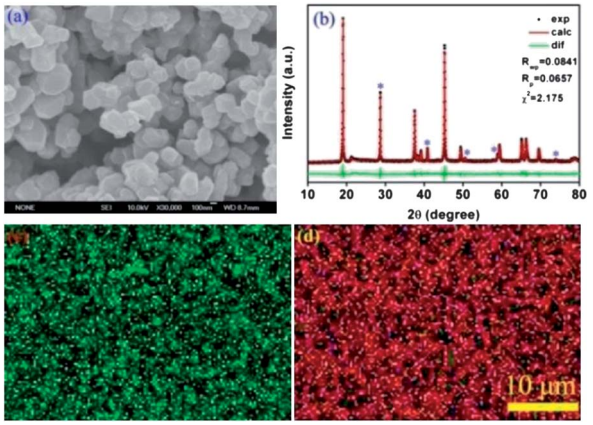

Fig. 4 (a) SEM image, (b) XRD pattern, and X-ray map results of (c) Mn and (d) Co for the synthesised $Li_{1.2}Mn_{0.4}Co_{0.4}O_2$ material.

layered $LiCoO_2$, while the weak peaks at 20–25° correspond to an integrated monoclinic $Li[Li_{1/3}Mn_{2/3}]O_2$ phase ($C2/m$) with cation ordering between the Li and the transition metal layer.[12] Careful XRD data examination also shows that the pair reflections (006)/(012) and (018)/(110) for $Li_{1.2}Mn_{0.4}Co_{0.4}O_2$ were well separated, and the intensity ratios $I_{(003)}/I_{(104)}$ and $I_{(101)}/[I_{(006)} + I_{(012)}]$ were 1.23 and 0.427. All these factors indicate that the sample had a high crystallinity, good hexagonal ordering, and layered characteristics.[13] The lattice parameters for the sample determined by Rietveld refinement were $a = 2.8327(1)$ and $c = 14.2125(4)$ Å for the layered $R\bar{3}m$ structure. The axis ratio c/a was 5.0173, slightly larger than that of 4.899 reported previously.[13] The molar ratio Li : Mn : Co determined by ICP-AES was 1.18 : 0.41 : 0.40, which is very closer to the target ratio. The XRD and ICP results demonstrate that a $Li_{1.2}Mn_{0.4}Co_{0.4}O_2$ cathode material with a good layered structure was successfully synthesized by the oxalate-precursor method. The almost uniform brightness of the X-ray map indicates a uniform cation distribution inside our synthesized material, as shown in Fig. 4c and d.

The oxidation states of the metal ions in the sample were determined by XPS, which showed the presence of the metal elements Mn, Co, and Li only (not shown). Core level XPS spectra of Mn 2p and Co 2p are illustrated in Fig. 5a and b. For Mn 2p, spin-orbit splitting peaks of 2p 3/2 and 2p 1/2 are clearly seen at 642.15 and 653.5 eV without any satellite peak, which indicates that the manganese ions were predominantly tetravalent.[14] In comparison, four signals were detected for the Co 2p

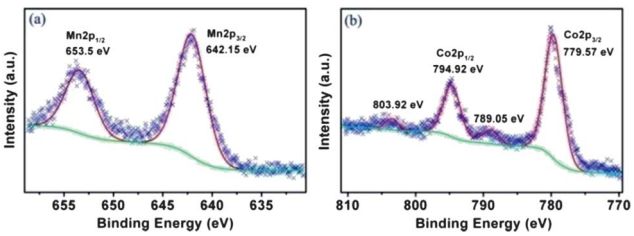

Fig. 5 XPS results for $Li_{1.2}Mn_{0.4}Co_{0.4}O_2$: (a) Mn 2p and (b) Co 2p.

core level: two strong signals at 779.57 and 794.92 eV correspond to the core levels of Co $2p_{3/2}$ and Co $2p_{1/2}$, while the other two weak signals located at 789.05 and 803.92 eV are their shake-up satellite peaks, which demonstrates that the Co ions were in an oxidation state of +3.[15]

The room-temperature electrochemical performance of the sample was first examined in a voltage window between 2.0 and 4.6 V at different current densities, as shown in Fig. 6. All the initial charge curves clearly displayed a smooth voltage ramp in the range 3.9–4.36 V, a long flat plateau in the range 4.36–4.55 V, and a small slope when charged above 4.55 V. The smooth voltage ramp can be ascribed to Li^+ de-intercalation from the layered $LiCoO_2$ structure, while the long flat plateau can be attributed to the oxygen loss process from the Li_2MnO_3 component which led to a large initial irreversible capacity loss.[16–18] The small slope may be due to electrolyte oxidation.[19] As indicated in Fig. 6a, upon lowering the current density from 200 to 20 mA g^{-1}, the initial charge capacity increased from 302 to 373 mA h g^{-1}, and the initial discharge capacity was enhanced, increasing from 203 to 284 mA h g^{-1}. In comparison, the coulombic efficiency slightly increased from 67 to 76%.

Redox reactions in the $Li_{1.2}Mn_{0.4}Co_{0.4}O_2$ cathode were examined using the corresponding differential capacity (dQ/dV) *vs.* voltage profiles, as shown in Fig. 6b. All the curves exhibited similar redox peaks, while the intensity and position of these peaks were highly dependent on the current density. For example, the oxidation peaks in a particular voltage region moved towards higher voltages, while the reduction peaks shifted towards lower voltages with increasing charge–discharge current density, indicating an enhancement of the polarization. The oxidation peak at approximately 4.01 V is ascribed to the $Co^{3+}/Co^{3.6+}$ oxidation process, and that at about 4.36 V is ascribed to the $Co^{3.6+}/Co^{4+}$ oxidation reaction, as observed in other work.[20] The very intense oxidation peak at about 4.47 V corresponds to the electrochemical activation of the Li_2MnO_3 component by its decomposition to Li_2O and MnO_2.[19,21] Since the activation reaction was highly irreversible, no corresponding reduction peak is observed in the initial discharge profile, but it induced a reduction reaction of $Mn^{4+} \rightarrow Mn^{3+}$ resulting in a reduction peak at around 3.3 V.[22] Additionally, the reduction peak in the 3.88 V region is apparently due to the reduction of Co^{4+}.[23,24]

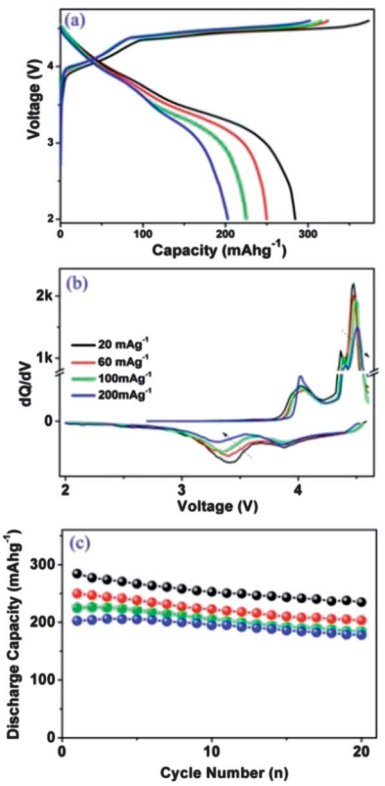

Fig. 6 Electrochemical performances measured at room-temperature (25 °C) for the $Li_{1.2}Mn_{0.4}Co_{0.4}O_2$ sample: (a) initial charge–discharge profiles at different current densities between 2.0 and 4.6 V, (b) corresponding plots of differential capacity *vs.* voltage, and (c) discharge capacity *vs.* cycle number curves.

As indicated in Fig. 6c, after 20 cycles, the discharge capacity of the $Li_{1.2}Mn_{0.4}Co_{0.4}O_2$ electrode still remained at 235 mA h g^{-1} at a current density of 20 mA g^{-1}, larger than the retained capacity of 195 mA h g^{-1} reported by Wei *et al.*,[25] which indicates that the cycling performance of the $Li_{1.2}Mn_{0.4}Co_{0.4}O_2$ cathode material was enhanced. Even when the current density was increased to 200 mA g^{-1}, the $Li_{1.2}Mn_{0.4}Co_{0.4}O_2$ electrode exhibited an initial discharge capacity as high as 203 mA h g^{-1}, and still displayed a discharge capacity larger than 178 mA h g^{-1} after 20 cycles. These results demonstrate that the $Li_{1.2}Mn_{0.4}Co_{0.4}O_2$ cathode synthesized by our oxalate-precursor method possessed a superior electrochemical performance at room temperature, which is barely accessible when using other synthetic methods.

Our sample also showed an excellent electrochemical behavior at an elevated temperature of 45.4 °C or at a low temperature of −10.4 °C. Fig. 7 shows the high-temperature electrochemical performance of the $Li_{1.2}Mn_{0.4}Co_{0.4}O_2$ cathode material measured at 45.4 °C between 2.0 and 4.6 V. Almost identically to the charge curve at room-temperature (Fig. 6a), the initial charge process recorded at 45.4 °C in Fig. 7a also consisted of three parts: a smooth voltage ramp, a long flat plateau, and a small slope, which demonstrates that the initial charge process remained essentially unchanged when the test temperature was increased. Nevertheless, at 45.4 °C, the first charge and discharge capacities at a current density of 20 mA g^{-1} were increased to 374 and 296 mA h g^{-1}, respectively. After 20 cycles, the charge and discharge capacities were still as large as 260 and 252 mA h g^{-1}.

Fig. 7b shows the differential capacity *vs.* voltage curves. It can be seen that the dQ/dV curve of the initial charge process displayed three oxidation peaks, identical to the room temperature dQ/dV curve in Fig. 6b. For the initial discharge process, the dQ/dV curve exhibited a large broad hump in the voltage range 2.5 to 4.2 V, which indicates that a spinel-like structure and a $LiMnO_2$ component emerged in the discharge process. In contrast to the initial charge process, two new oxidation peaks were clearly observed at 3.06 and 3.34 V in the subsequent cycling process. Both oxidation peaks can be attributed to Li^+ de-intercalation from the spinel-like structure (*i.e.*, in the 3.06 V region) and layered $LiMnO_2$ structure (*i.e.*, in the 3.34 V region).

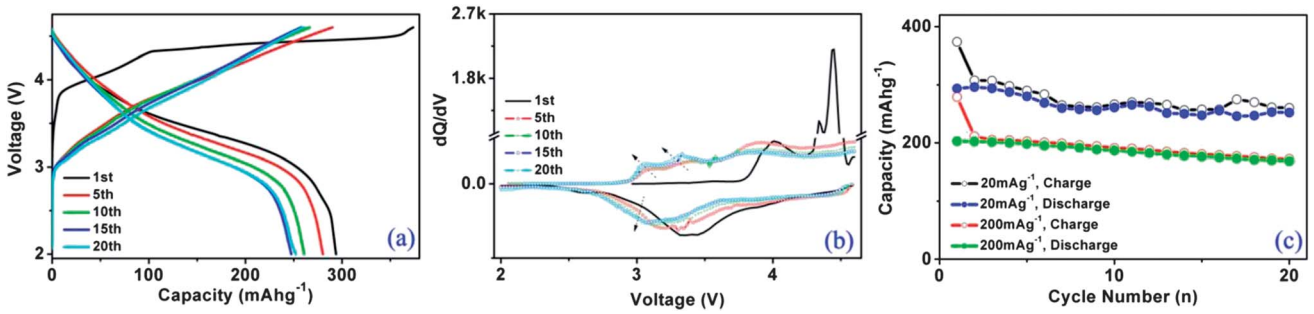

Fig. 7 Electrochemical performances measured at the high temperature of 45.4 °C for $Li_{1.2}Mn_{0.4}Co_{0.4}O_2$: (a) charge–discharge profiles of different cycles at 20 mA g^{-1} between 2.0 and 4.6 V, (b) the corresponding differential capacity *vs.* voltage curves, and (c) capacity *vs.* cycle number plots at current densities of 20 and 200 mA g^{-1}.

As shown in Fig. 7b, as the cycle number increased, all oxidation and reduction peaks moved towards lower voltages. Noticeably, the intensities of the oxidation and reduction peaks in the 3.06 and 3.34 V regions increased with cycling, which indicates that the contents of the spinel-like structure and layered $LiMnO_2$ structure components in the electrode increased with cycling. In other words, the content of Mn^{3+} increased with cycling at elevated temperatures.

Fig. 7c shows the high temperature capacity *vs.* cycle number plots at 20 and 200 mA g^{-1} measured at 45.4 °C. It can be seen that even at a current density of 200 mA g^{-1}, the sample showed a good capacity. The initial charge and discharge capacities were 279 and 203 mA h g^{-1}, and were maintained as high as 172 and 169 mA h g^{-1} after 20 cycles. Based on the discussion of Fig. 7b, the slight capacity fading with cycling could be related to the increase of Jahn–Teller active Mn^{3+} ions.

The low-temperature electrochemical performance of the $Li_{1.2}Mn_{0.4}Co_{0.4}O_2$ cathode material tested at −10.4 °C between 2.0 and 4.6 V is illustrated in Fig. 8. Fig. 8a displays the charge–discharge profiles measured during the 1st, 10th, 20th, 30th, and 40th charge–discharge cycles. The initial charge curve only consisted of two electrochemical processes as displayed by a smooth voltage ramp and a long flat plateau. The small slope corresponding to the electrolyte oxidation process at voltages above 4.55 V is absent. The initial charge and discharge capacities at a current density of 20 mA g^{-1} were 298 and 170 mA h g^{-1}. More importantly, after 40 cycles, the capacity was still greater than 202 mA h g^{-1} for the charge process and 193 mA h g^{-1} for the discharge process without any capacity loss. Upon carefully examining the initial charge curves recorded at a current density of 20 mA g^{-1} in Fig. 6a, 7a and 8a, it can be seen that the charge capacity in the smooth voltage ramp region was 101 mA h g^{-1} at 45.4 °C, while those at 25 °C and −10.4 °C were maintained at 99 mA h g^{-1}. The fact that the capacities were very close for these test temperatures is surprising, since the amount of Li^+ de-intercalated from the layered component in the voltage window 2.0–4.6 V is determined to be independent of the test temperature.

For the purposes of comparison, the charge capacities for the long flat plateau for the three test temperatures were 263 mA h g^{-1} at 45.4 °C, 259 mA h g^{-1} at 25 °C, and 198 mA h g^{-1} at −10.4 °C. It appears that decreasing the test temperature was unhelpful for the electrochemical activation of the Li_2MnO_3 component. Therefore, for the present $Li_{1.2}Mn_{0.4}Co_{0.4}O_2$ composite, upon increasing the degree of electrochemical activation of the Li_2MnO_3 component, the capacity properties of the composite cathode material would be improved.

To further study the effects of temperature on the electrochemical performance of $Li_{1.2}Mn_{0.4}Co_{0.4}O_2$ electrodes, the corresponding dQ/dV derivative plots for the 1st, 10th, 20th, 30th, and 40th charge–discharge cycles and the cycling performances were also recorded. As shown in Fig. 8b, the dQ/dV curves were different from those shown in Fig. 6b and 7b. First, the dQ/dV curve of the initial charge process only exhibits two oxidation peaks at 4.15 and 4.52 V, corresponding to the oxidation of the

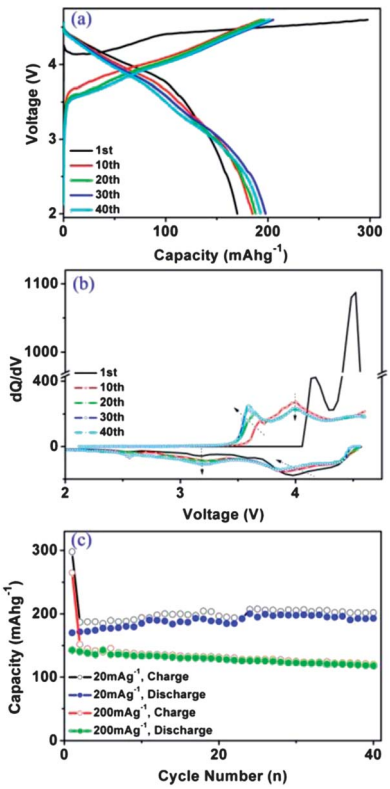

Fig. 8 Electrochemical performance at a low-temperature of −10.4 °C for $Li_{1.2}Mn_{0.4}Co_{0.4}O_2$: (a) charge–discharge profiles of different cycles at 20 mA g^{-1} between 2.0 and 4.6 V, (b) corresponding differential capacity *vs.* voltage curves, and (c) capacity *vs.* cycle number plots at 20 and 200 mA g^{-1}.

layered $LiCoO_2$ structure and the loss of oxygen (from Li_2MnO_3), respectively. Upon comparing with the data at 45.4 °C (Fig. 7b), the oxidation peaks for all the charge processes moved towards higher voltages, while the corresponding reduction peaks shifted obviously towards lower voltages, which demonstrates that the polarization of the $Li_{1.2}Mn_{0.4}Co_{0.4}O_2$ electrodes increased upon decreasing the working temperature. Second, the dQ/dV curves for the 10th, 20th, 30th and 40th charge processes only displayed two oxidation peaks in the 3.6 and 4.0 V regions. The absence of an oxidation peak at about 3 V indicates that hardly any of the spinel-like structure was produced during the cycling process. This should be related to fact that only some of the Li_2MnO_3 was activated and the content of MnO_2 in the cathode was not high enough for the formation of the spinel-like oxide structure during the charge–discharge process. Third, the reduction peak representing the production of the spinel-like structure cannot be observed except for in the 30th discharge process. This is because the degree of electrochemical activation of the Li_2MnO_3 was low which caused the content of MnO_2 in the cathode material to be too little for the production of the spinel-like structure.

Fig. 8c shows the low-temperature (−10.4 °C) cycling performance profiles at 20 and 200 mA g^{-1}. The initial charge and discharge capacities were 265 and 142 mA h g^{-1} at a current density of 200 mA g^{-1}. After 40 cycles, the discharge capacity was still as high as 118 mA h g^{-1} which delivered a capacity retention ratio of 83.1%. It is worth saying that the discharge capacity hardly faded with cycling and achieved a maximum as high as 200 mA h g^{-1} in the 24th cycle. The better cycle performance at −10.4 °C is likely to be closely related to the absence of the spinel-like oxide structure during the charge–discharge process as evidenced by the dQ/dV curves in Fig. 8b. From the discussion above (regarding Fig. 6–8), it can be concluded that upon increasing the temperature, the degree of electrochemical activation of the Li_2MnO_3 component was enhanced, giving rise to a greater amount of Jahn–Teller active Mn^{3+} ions or spinel-like structure during the subsequent discharge process. That is, during the discharge process, the amount of Li^+ intercalated in the composite electrode was increased at elevated temperatures to give a superior discharge capacity. As a result, a high concentration of Mn^{3+} occurred, according to the following disproportionation reaction:[25]

$$2Mn^{3+} \rightarrow Mn^{4+} + Mn^{2+} \quad (1)$$

In this reaction, transition metal Mn^{2+} ions would have been dissolved in the electrolyte, resulting in a gradual capacity decay. This may explain why the $Li_{1.2}Mn_{0.4}Co_{0.4}O_2$ electrode possessed superior capacity properties and a relatively poor cycling life when the cells were measured at the elevated-temperature of 45.4 °C.

To investigate the electrode kinetics, electrochemical impedance spectroscopy (EIS) was carried out on the $Li_{1.2}Mn_{0.4}Co_{0.4}O_2$/Li cells which were initially charged to 4.6 V at different temperatures. Impedance is a collective response of kinetic processes that respond in different time regimes. Fig. 9 presents the Nyquist plots of the $Li_{1.2}Mn_{0.4}Co_{0.4}O_2$ electrode tested from 100 kHz to 10 mHz and the corresponding profiles of the real part of the impedance (Z_r) *vs.* $\omega^{-1/2}$ in the frequency region 0.1–0.01 Hz which is used to calculate the Warburg factor. The impedance spectra were analyzed by Zsimpwin software and the data fitted to the equivalent circuit shown in the inset of Fig. 9a.

Here, R_e represents the internal resistance of the cell, R_{sf} and C_{sl} are the resistance and capacitance of the solid electrolyte interphase (SEI) film, R_{ct} and C_{dl} are the charge transfer resistance and double layer capacitance, and W is the Warburg impedance that is directly related to the lithium ion diffusion process in the electrode.

The formation of the SEI film on the $Li_{1.2}Mn_{0.4}Co_{0.4}O_2$ cathode electrodes involves a series of spontaneous reactions between the cathode active materials and the electrolyte solvents. First, the SEI film can greatly reduce the electronic conductivity of the $Li_{1.2}Mn_{0.4}Co_{0.4}O_2$ particles and cause an irreversible capacity loss.[26] Second, the SEI film should form a passivating layer that is compact to prevent the penetration of the electrolyte and the solvated Li compounds and should be sufficiently ionically conductive to permit the reversible intercalation/de-intercalation of Li^+ ions. All these factors can enhance the cycle performance of the $Li_{1.2}Mn_{0.4}Co_{0.4}O_2$ cathode electrodes.[27] It is well documented that the contributions of different solvents (EC, EMC and DMC) to SEI film formation are not equal, as indicated by literature reports eleswhere.[28] EC plays a major role in SEI film formation, while EMC and DMC contribute little. The contribution could decrease in the sequence, EC > EMC > DMC.

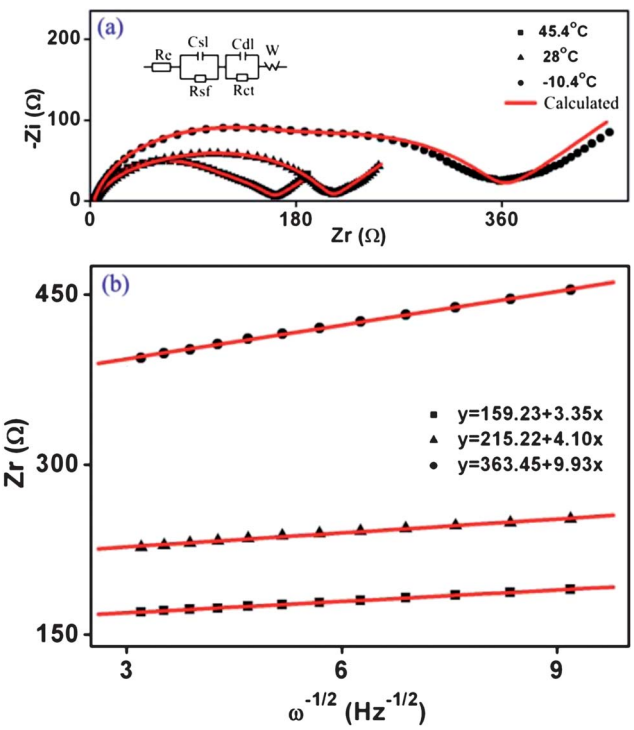

Fig. 9 (a) Electrochemical impedance spectra of $Li_{1.2}Mn_{0.4}Co_{0.4}O_2$/Li cells recorded at room temperature and charged to 4.6 V during the 1st cycle, and (b) the profiles of Z_r *vs.* $\omega^{-1/2}$ from 0.1 Hz to 0.01 Hz.

As shown in Fig. 9a, all Nyquist plots exhibit an arc in the high frequency region and a slope in the low frequency region, with the arc being composed of two semicircles. The intercept of the arc at the highest frequency with the real axis (Z_r) represents the uncompensated ohmic resistance between the working electrode and the reference electrode, and the diameters of the two semicircles obtained by Zsimpwin software represent the resistance of the surface film (R_{sf}) and the charge transfer resistance (R_{ct}).

The values for R_e, R_{sf}, R_{ct}, and R_{total} (total resistance) are shown in Table 1, from which we can find that the total resistance and R_{sf} greatly increased as the temperature decreased to −10.4 °C. This indicates that the Li^+ ions find it more and more difficult to pass through the SEI film and electrode as the temperature is decreased.

The slope in Fig. 9a is attributed to the diffusion of lithium ions into the bulk of the electrode material, which is called Warburg diffusion. The diffusion coefficient of lithium ions can be calculated from the slope in the low-frequency region according to the following equation,[15,29]

$$D_{Li+} = 0.5R^2T^2/n^4A^2F^4C^2\sigma^2 \quad (2)$$

where R is the ideal gas constant, T is the absolute temperature, n is the number of electrons per molecule oxidized, A is the surface area of the electrode, F is the Faraday constant, C is the concentration of Li^+ in the cathode, and σ is the Warburg factor which is related to Z_r as follows:

$$Z_r = R_e + R_{sf} + R_{ct} + \sigma\omega^{-0.5} \quad (3)$$

from which σ can be obtained from the linear fit of Z_r *vs.* $\omega^{-0.5}$. Fig. 9b shows the relationship between Z_r and the reciprocal square root of the frequency in the low-frequency region from 0.1 Hz to 0.01 Hz recorded at −10.4, 28, and 45.4 °C. The diffusion coefficients of the lithium ions in the $Li_{1.2}Mn_{0.4}Co_{0.4}O_2$ electrode recorded at −10.4, 28, and 45.4 °C were calculated according to eqn (2), and were 8.8797×10^{-16}, 6.8424×10^{-15}, and 1.1468×10^{-14} cm^2 s^{-1} in the initial full charge state, respectively. It is clear that the diffusion coefficient of the lithium ions increased with increasing temperature, and the difference between the diffusion coefficients at adjacent temperatures is about one order of magnitude.

It should be mentioned that lithium-rich materials have been previously prepared by a conventional co-precipitation method. The materials thus prepared usually exhibit a certain uniform distribution of cations on the micro scale, while cation segregation may exist in local domains.[30] As a result, the electrochemical performances are always unsatisfactory at elevated/low temperatures.[31] For our lithium-rich samples, the electrochemical performances at elevated/low temperatures were pretty good, which was most likely due to the uniform cation distribution as indicated by the X-ray mapping data in Fig. 4. Further investigation is essential to study the cation local domains for our lithium-rich samples. From the above discussion, we can conclude that the $Li_{1.2}Mn_{0.4}Co_{0.4}O_2$ material synthesized by our method possessed a large diffusion coefficient, which was a consequence of the uniform mixing of the reactants at the molecular level. This may also explain why our sample exhibited excellent electrochemical performances from −10.4 to 45.4 °C.

To estimate the SOH of the $Li_{1.2}Mn_{0.4}Co_{0.4}O_2$/Li cells, EIS was performed as follows: (i) the first EIS was obtained when the cell was charged to 4.6 V (full charge) after four charge–discharge cycles at room temperature; (ii) the cell was moved to a thermostatic chamber at −10.4 °C and discharged to 2.0 V, and then charged to 4.6 V at room temperature to get a second EIS after four charge–discharge cycles in the thermostatic chamber; (iii) the cell was moved to a thermostatic chamber at 45.4 °C and discharged to 2.0 V, and then, to acquire a third EIS, the cell was charged to 4.6 V at room temperature after four charge–discharge cycles in the thermostatic chamber; (iv) in order to get a fourth EIS, the cell was tested at room temperature until the 20th full charge. We used the change in the impedance with cycle number (number of charge–discharge cycles in the temperature range investigated) to assess the %SOH change of the $Li_{1.2}Mn_{0.4}Co_{0.4}O_2$/Li cells. The %SOH change over the temperature range used was investigated by EIS. As shown in Fig. 10, the total impedances for the 5th full charge, 10th full charge, 15th full charge, and 20th full charge were 536.6, 549.8, 458.2, and 458.2 Ω, respectively. It was easy to find that the % SOH changes in the temperature range from −10.4 to 45.4 °C were distributed in a range from 2.46% to −14.61%. The impedance of the cell increased when the working temperature of the cell was changed from room temperature to −10.4 °C, and then decreased when the cell was cycled at 45.4 °C. Eventually, the impedance remained almost stable at 458.2 Ω. This result indicates that the %SOH operation window of the $Li_{1.2}Mn_{0.4}Co_{0.4}O_2$/Li cells was somewhat broad, demonstrating

Table 1 Parameters for EIS obtained using Zsimpwin software

	Temperature (°C)		
R	−10.4	28	45.4
R_e (Ω)	3.229	3.821	5.145
R_{sf} (Ω)	197.5	157.6	77.12
R_{ct} (Ω)	153.7	47.89	77.99
R_{total} (Ω)	354.4	209.3	160.3

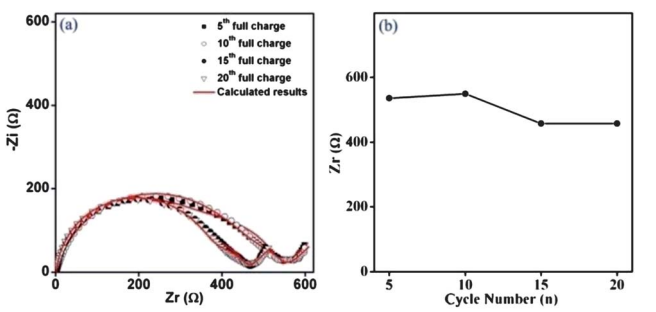

Fig. 10 EIS of $Li_{1.2}Mn_{0.4}Co_{0.4}O_2$/Li cells carried out during the 5th full charge (charged to 4.6 V), 10th full charge, 15th full charge, and 20th full charge at room temperature.

a great potential application as an electrode material at low/elevated temperatures.

4 Conclusions

We have successfully synthesized $Li_{1.2}Mn_{0.4}Co_{0.4}O_2$ by a new oxalate-precursor method. When compared to the previous co-precipitation methods, this method greatly improves the uniform distribution of the reactants, which means the cations are distributed uniformly inside the materials. When tested as a cathode for lithium-ion batteries, the resulting $Li_{1.2}Mn_{0.4}Co_{0.4}O_2$ material exhibited an excellent electrochemical performance over the temperature range −10.4 to 45.4 °C. At a current density of 20 mA g^{-1}, the maximum discharge capacities were 296, 284, and 200 mA h g^{-1}, at 45.4, 28, and −10.4 °C, respectively. Even at a current density of 200 mA g^{-1}, the initial discharge capacities were still as large as 203, 203, and 142 mA h g^{-1}, respectively. The EIS results indicate that the %SOH operation window in the temperature range investigated is somewhat broad, which is helpful for the application of the $Li_{1.2}Mn_{0.4}Co_{0.4}O_2$ cathode material at low/elevated temperatures. The synthetic method reported here may be extended to other advanced metal-oxide cathode materials of lithium-ion batteries for application in a wide temperature range.

Acknowledgements

This work was financially supported by the NSFC (21025104, 91022018 and 21271171), the National Basic Research Program of China (2011CB935904), and FJIRSM funds (SZD08002-3 and SZD09003-1).

Notes and references

1 Y.-K. Sun, B.-R. Lee, H.-J. Noh, H. Wu, S.-T. Myung and K. Amine, *J. Mater. Chem.*, 2011, **21**, 10108.
2 H. Li and H. Zhou, *Chem. Commun.*, 2012, **48**, 1201.
3 C. Yu, X. Guan, G. Li, J. Zheng and L. Li, *Scr. Mater.*, 2012, **66**, 300.
4 D. Li, T. Muta and H. Noguchi, *J. Power Sources*, 2004, **135**, 262.
5 C. Yu, G. Li, X. Guan, J. Zheng and L. Li, *J. Alloys Compd.*, 2012, **528**, 121.
6 T. A. Arinkumar, Y. Wu and A. Manthiram, *Chem. Mater.*, 2007, **19**, 3067.
7 Y. Jiang, Z. Yang, W. Luo, X. L. Hu, W. X. Zhang and Y. H. Huang, *J. Mater. Chem.*, 2012, **22**, 14964.
8 N. Tran, L. Croguennec, M. Menetrier, F. Weill, P. Biensan, C. Jordy and C. Delmas, *Chem. Mater.*, 2008, **20**, 4815.
9 J. R. Croy, M. Balasubramanian, D. Kim, S.-H. Kang and M. M. Thackeray, *Chem. Mater.*, 2011, **23**, 5415.
10 T.-H. Cho, Y. Shiosaki and H. Noguchi, *J. Power Sources*, 2006, **159**, 1322.
11 D. Luo, G. Li, C. Yu, L. Yang, J. Zheng, X. Guan and L. Li, *J. Mater. Chem.*, 2012, **22**, 22233.
12 R. Santhanam, P. Jones, A. Sumana and B. Rambabu, *J. Power Sources*, 2010, **195**, 7391.
13 T. Mei, K. Tang, Y. Zhu and Y. Qian, *Dalton Trans.*, 2011, **40**, 7645.
14 J. K. Ngala, N. A. Chernova, M. M. Ma, M. Mamak, P. Y. Zavalij and M. S. Whittingham, *J. Mater. Chem.*, 2004, **14**, 214.
15 J. Y. Xiang, J. P. Tu, Y. Q. Qiao, X. L. Wang, J. Zhong, D. Zhang and C. D. Gu, *J. Phys. Chem. C*, 2011, **115**, 2505.
16 S.-H. Kang, W. Lu, K. G. Gallagher, S.-H. Park and V. G. Pol, *J. Electrochem. Soc.*, 2011, **158**, A936.
17 F. Zhou, X. Zhao, A. van Bommel, X. Xia and J. R. Dahn, *J. Electrochem. Soc.*, 2011, **158**, A187.
18 F. Amalraj, D. Kovacheva, M. Talianker, L. Zeiri, J. Grinblat, N. Leifer, G. Goobes, B. Markovsky and D. Aurbach, *J. Electrochem. Soc.*, 2010, **157**, A1121.
19 M. M. Thackeray, C. S. Johnson, J. T. Vaughey, H. N. Li and S. A. Hackney, *J. Mater. Chem.*, 2005, **15**, 2257.
20 W. He, J. Qian, Y. Cao, X. Ai and H. Yang, *RSC Adv.*, 2012, **2**, 3423.
21 J. Li, R. Klöpsch, S. Nowak, M. Kunze, M. Winter and S. Passerini, *J. Power Sources*, 2011, **196**, 7687.
22 F. Wu, N. Li, Y. Su, H. Lu, L. Zhang, R. An, Z. Wang, L. Bao and S. Chen, *J. Mater. Chem.*, 2012, **22**, 1489.
23 J.-M. Kim, S. Tsuruta and N. Kumagai, *Electrochem. Commun.*, 2007, **9**, 103.
24 H. Porthault, F. L. Cras, R. Baddour-Hadjean, J. P. Pereira-Ramos and S. Franger, *Electrochim. Acta*, 2011, **56**, 7580.
25 Z. Li, Y. Wang, X. Bie, K. Zhu, C. Wang, G. Chen and Y. Wei, *Electrochem. Commun.*, 2011, **13**, 1016.
26 S. S. Zhang, K. Xu and T. R. Jow, *J. Electrochem. Soc.*, 2002, **149**, A1521.
27 F. Kong, R. Kostecki, G. Nadeau, X. Song, K. Zaghib, K. Kinoshita and F. McLarnon, *J. Power Sources*, 2001, **97**, 58.
28 Y. Wang and P. B. Balbuena, *Int. J. Quantum Chem.*, 2005, **102**, 724.
29 Q. Cao, H. P. Zhang, G. J. Wang, Q. Xia, Y. P. Wu and H. Q. Wu, *Electrochem. Commun.*, 2007, **9**, 1228.
30 D. Wang, I. Belharouak, S. Gallagher, G. Zhou and K. Amine, *J. Mater. Chem.*, 2012, **22**, 12039.
31 A. V. Churikov, *Electrochim. Acta*, 2001, **46**, 2415.